Effects of Laser Bandwidth in Direct-Drive High-Performance DT-Layered Implosions on the OMEGA Laser

D. Patel[1,2] J. P. Knauer,[1] D. Cao,[1] R. Betti,[1,2,3] R. Nora,[4] A. Shvydky,[1] V. Gopalaswamy,[1] A. Lees,[1] S. Sampat,[1] W. R. Donaldson,[1] S. P. Regan,[1] C. Stoeckl,[1] C. J. Forrest,[1] V. Yu. Glebov,[1] D. R. Harding,[1] M. J. Bonino,[1] R. T. Janezic,[1] D. Wasilewski,[1] C. Fella,[1] C. Shuldberg,[5] J. Murray,[5] D. Guzman,[5] and B. Serrato[5]

[1]Laboratory for Laser Energetics, University of Rochester, New York 14623, USA
[2]Department of Mechanical Engineering, University of Rochester, New York 14623, USA
[3]Department of Physics and Astronomy, University of Rochester, New York 14623, USA
[4]Lawrence Livermore National Laboratory, Livermore, California 94550, USA
[5]General Atomics, San Diego, California 92186, USA

In direct-drive inertial confinement fusion, the laser bandwidth reduces the laser imprinting seed of hydrodynamic instabilities. The impact of varying bandwidth on the performance of direct-drive DT-layered implosions was studied in targets with different hydrodynamic stability properties. The stability was controlled by changing the shell adiabat from ($\alpha_F \simeq 5$) (more stable) to ($\alpha_F \simeq 3.5$) (less stable). These experiments show that the performance of lower adiabat implosions improves considerably as the bandwidth is raised indicating that further bandwidth increases, beyond the current capabilities of OMEGA, would be greatly beneficial. These results suggest that the future generation of ultra-broadband lasers could enable achieving high convergence and possibly high gains in direct drive ICF.

In laser-driven inertial confinement fusion (ICF) [1–3], a spherical shell (ablator) with an inner deuterium-tritium ice layer is accelerated inward to high velocities of hundreds of km/s to achieve, upon stagnation, the conditions of density and temperature required for thermonuclear ignition. In laser-direct-drive (LDD) ICF [4], the ablation pressure from the direct illumination of the shell is the mechanism driving the implosion. The ablation pressure is produced by the rocket effect from mass ablation off the shell outer surface (the ablation front). During the target acceleration, the low-density ablated plasma pushes on the dense shell, thus making the ablation front unstable to the Rayleigh-Taylor instability (RTI) [5,6]. Small-scale variations in the laser irradiation (speckles) produce ablation pressure perturbations resulting in surface nonuniformities known as "laser imprinting" [7–9]. Laser imprinting occurs during the initial interaction of the laser light with the target surface when the ablated plasma is still tenuous and the perturbations in ablation pressure are felt by the target. Once a large plasma atmosphere is established with a critical surface distance D_c from the ablation front, all short-wavelength perturbations with wave number $k > 1/D_c$ are damped by thermal conduction and imprinting ceases to occur. The surface nonuniformities from laser imprinting act as seeds for the Rayleigh-Taylor instability. The RTI growth of these perturbations can severely degrade the integrity of the imploding shell, thus reducing the final compression and preventing ignition. Imprint mitigation is considered critical in achieving ignition with LDD. To that intent, various beam smoothing techniques have been developed [10–18]. Nominal OMEGA cryogenic implosions use distributed-phase plates (DPPs) [14,19] and smoothing by spectral dispersion (SSD) [12,13] to improve the laser uniformity [20,21]. Past experiments were designed to study specific aspects of imprinting growth [22–28]. For instance, burn-through experiments in both planar [23–25] and spherical geometry [26] were performed to investigate the depth of the RT bubble front seeded by imprinting. Implosion experiments on warm surrogate plastic shells were fielded with full SSD smoothing [28] to study degradations at different adiabats. None of these experiments can inform on the effects of imprinting in ICF-relevant DT-layered implosions which exhibit vastly different stability properties with respect to warm plastic shells. Furthermore, varying the imprinting seed for a fixed laser pulse shape is a much cleaner way to isolate and probe the effect of imprinting. Here we report on the first experimental campaign aimed at assessing the performance of cryogenic DT-layered implosions as a function of laser smoothing. The SSD smoothing is varied by changing OMEGA laser bandwidth $\Delta\nu_{UV}$ from approximately 0 to the maximum value of ~355 GHz (1 THz equivalent with three color cycles [29]). An important outcome of these experiments is a quantitative assessment of the benefits of laser bandwidth on implosion performance. Data acquired at different bandwidth also provides the basis for extrapolating the results to bandwidths higher than currently achievable on OMEGA. Such an extrapolation is critical in motivating
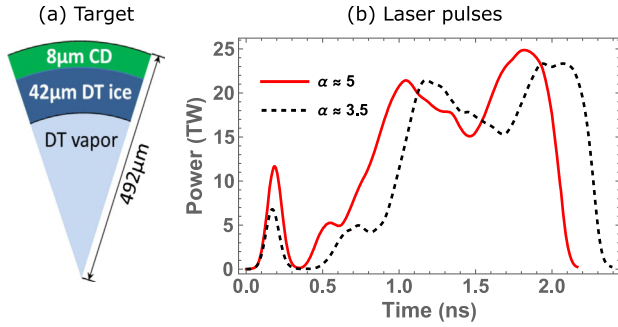
FIG. 1.   (a) Target geometry for cryogenic SSD-scan implosions. Variation in outer diameter was ± 5 μm, CD ablator thickness varied to within ± 0.4 μm. (b) Laser pulses for the $\alpha_F \simeq 3.5$ (in black dashed) and $\alpha_F \simeq 5$ (in solid red) baseline implosions.

TABLE I.   1D (LILAC) calculated design parameters and performance metrics for nominal (100% SSD) implosions.

α_F	IFAR	V_{imp} (km/s)	Convergence ratio	Total yield	ρR (mg/cm^2)
5	22	457	17	4.1×10^{14}	187
3.5	31	462	19	5×10^{14}	206

the development of broadband lasers for high-gain direct-drive ICF [30,31] and other imprint mitigation techniques [32,33].

The bandwidth scan was carried out for two fixed laser pulse shapes designed to keep the minimum adiabat α_F at 3.5 (low adiabat) and 5 (high adiabat). Here $\alpha_F = P/P_{\text{Fermi}}$ is the ratio of the plasma pressure to the Fermi degenerate pressure in-flight at about 2/3 of the inner radius. The targets are from previous designs that achieved record performance at $\alpha_F \approx 5$ [34]. The main performance metrics for DT-layered implosions are the fusion yields and the areal densities which determine the no-alpha Lawson parameter $\chi_{\text{no}-\alpha}$ [35,36] with the ignition threshold set at $\chi_{\text{no}-\alpha} \approx 0.96$–1. Equivalent metrics such as $ITFx$ [37] and f_α [38] can also be used to measure proximity to ignition.

Figure 1 shows the target and laser pulses used for these experimental campaigns. Targets have a CD ablator of ~8 μm, DT ice layer of ~42 μm and total outer diameter of ~980 μm with the exception of one shot where ~3 μm silicated plastic [CH-Si(6%)] outer layer with ~4 μm inner CH layer were used. Targets were layered with 40%–60% (D–T) composition ice. Experiments employed 60-beams symmetric drive of OMEGA 351 nm UV laser, with SG5-850 DPP's leading to a beam diameter of 830 μm (enclosing 95% of the energy) and beam profile approximated by a super-Gaussian with an exponent ≈ 5. Pulse shapes use a picket and a foot to set the shell adiabat, followed by a ~2 ns "double-spike" main drive, with an average overlapped intensity of $\sim 7 \times 10^{14}$ W/cm^2. The total energy delivered to target is ~28.5 kJ.

Picket and foot power were lowered for $\alpha_F \simeq 3.5$ design to send weaker shocks through the shell. Lower adiabats lead to higher densities during the acceleration phase, resulting in thinner shells and higher aspect ratios in flight, making it more susceptible to the growth of short-scale perturbations. Both designs have similar laser drives during the acceleration phase, which results in similar implosion velocities. According to 1D simulations, $\alpha_F \simeq 3.5$ design shows higher DT neutron yield, and burn-averaged

areal density because of higher final convergence. These LILAC 1D [39] calculated quantities are shown in Table I for both designs. LILAC simulations include state-of-art physics models for cross-beam-energy transfer (CBET) [40,41], nonlocal heat transport [42], and first-principles equation-of-state (FPEOS) [43]. The hydrodynamic stability is expected to be degraded at lower adiabats resulting in higher growth of the RTI and deeper penetration of the RT bubble front into the imploding shell.

Table II shows the experimentally measured data denoting the performance of the implosions at full bandwidth. Note that measured yields have been corrected for mode $l = 1$ using measured ion temperature asymmetries [44,45]. The $\alpha_F \simeq 3.5$ implosions performed poorly compared to $\alpha_F \simeq 5$ implosions, with ~60% yield and ~80% of the areal density. Areal densities are measured along two different lines-of-sight using a neutron time-of-flight (nTOF) detector [46,47] and magnetic recoil spectrometer (MRS) [48,49]. The average of the two ρR is quoted. Inferred hot-spot radii from x-ray self-emission images from the gated monochromatic x-ray imager (GMXI) [50] and convergence ratios are similar for both designs. Statistical modeling attributes this yield degradation to the growth of short-wavelength modes during the acceleration phase [44,51], which is governed by the shell adiabat and in-flight aspect ratio. Note that this dependence is also justified by an independent theoretical analysis [52]. See the Supplemental Material [53] for details. Known sources of short-scale perturbations are target surface roughness, ablator defects produced by beta decay of tritium during filling and ice layering [56], and laser imprinting. Statistical models cannot differentiate among the different sources. As shown in the Supplemental Material [53], these models attribute ~10% yield degradation to short-scale perturbations for $\alpha_F \simeq 5$ and ~40% for $\alpha_F \simeq 3.5$ implosions with full SSD smoothing.

In these SSD-scan experiments, the laser bandwidth $\Delta \nu_{\text{UV}}$ was varied between ~0.355 and ~0.05 THz (0.355 THz $\equiv$ 100% SSD). Dedicated experiments with ≈ 100 ps picket intensity pulses (no main drive) were also performed to measure the variation in single beam intensity smoothing level with varying bandwidth, using ultraviolet equivalent-target-plane (UV-ETP) images [21]. In addition, on-shot bandwidth was measured using UVSPEC (UV spectrometer) [57]. Figure 2 shows single pixel intensity line-outs from UVETP images (denoting spatial variations

TABLE II. Experimentally measured performance metrics for nominal (100% SSD) implosions. Note: Yields are corrected for $l = 1$ asymmetries [44,45].

α_F	Yield	ρR (mg/cm^2)	R_{hs}(μm)	Convergence Ratio	Min. $\langle T_{\mathrm{ion}} \rangle_n$ (keV)
5	$1.29 \pm 0.1 \times 10^{14}$	145 ± 26	29.5 ± 0.1	14.3 ± 0.2	4.29 ± 0.3
3.5	$0.83 \pm 0.07 \times 10^{14}$	116 ± 18	29.0 ± 0.1	14.7 ± 0.2	3.95 ± 0.3

across the beam), for bandwidth of 0.355 THz in red and 0.15 THz in black.

The total on-target illumination nonuniformity σ_{rms} was calculated using hard sphere (no plasma) superposition of 60 such beam profiles, leading to $\sigma_{\mathrm{rms}} \simeq 20.3(\%)/\sqrt{47.5 \times \mathrm{SSD\_fraction} + 1}$. Note that, although reducing SSD bandwidth also degrades low and intermediate mode uniformity, primarily due to reduction in the beam waist (radius enclosing 95% energy) with decreasing SSD bandwidth, laser imprint modes ($l > 20$) dominate the total nonuniformity. Note that nonuniformity is not a linear function of SSD bandwidth and exhibits progressively diminishing smoothing as SSD bandwidth is increased. See the Supplemental Material [53] for details of non-uniformity calculations.

Next, we discuss implosion results from the SSD scans. To better visualize the trends, we normalize the measured values at each SSD bandwidth fraction to measured values at 100% SSD. Also, there are unintended small variations in laser pulse and target geometry resulting in small variations in 1D calculated yields (ρR variations in one dimension are negligible). Additionally, laser beam waist also varies by a small amount ($\approx 5\%$) with SSD bandwidth. We take into account the effects of these variations by normalizing yields to 1D calculated values for the respective experiment by defining YOC $\equiv Y_{\mathrm{Exp}}/Y_{\mathrm{1D}}$. If multiple shots are available at the same SSD bandwidth, we report an average of the measurements. Additionally, we observed ion-temperature asymmetries in a few of these experiments from a mode 1 perturbation. As shown in Refs. [44,45], the degradation from mode 1 can be

accurately quantified using the maximum and minimum apparent ion temperatures measured along six lines of sight. For ion-temperature ratios $R_T = T_{\max}/T_{\min} > 1.14$, yields can be corrected for a mode 1 degradation by $(R_T/1.14)^{1.37}$. Most likely, the mode 1 perturbation is not related to a specific implosion design but rather caused by a random source, such as target offset from target-chamber center, laser beam mispointing, or laser power imbalance which affect a specific shot or all experiments carried out on a specific day.

We first consider $\alpha_F \simeq 5$ SSD scan. Figure 3 shows the variation in the primary performance metrics, neutron yield, and areal density as the SSD bandwidth is varied. Experiments show no variation (beyond measurement uncertainty) in yield and areal density above the SSD bandwidth fraction of 40%, indicating that above $\sim 40\%$ SSD, there is no degradation from imprinting left to be mitigated. Figure 3 clearly shows that the $\alpha_F \simeq 5$ implosions would not benefit from higher bandwidth than currently available on OMEGA.

Next, we discuss results from $\alpha_F \simeq 3.5$ SSD scan. Figure 4 shows the observed trends in YOC and areal density with least-square-fits to the data. Both performance metrics begin to degrade as soon as the SSD bandwidth is lowered from 100% SSD. Trends are statistically significant at a 95% confidence interval, with reduced χ^2 statistics of 1.16 and 0.97, respectively. Observed sensitivity of the performance close to 100% SSD suggests a high likelihood that even at 100% SSD there is performance degradation
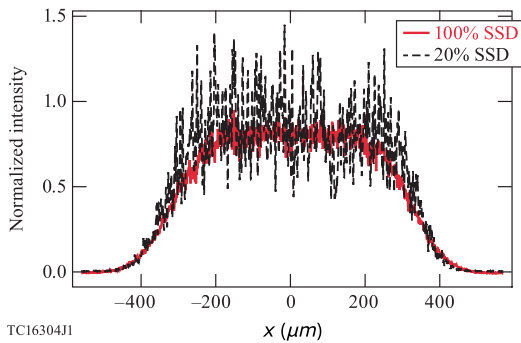

FIG. 2. Single pixel line-out from measured UVETP images for a single beam. Data are shown in red solid lines for 100% SSD and in black dashed lines for 20% SSD.
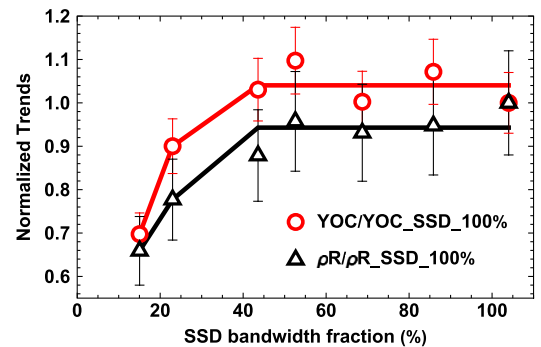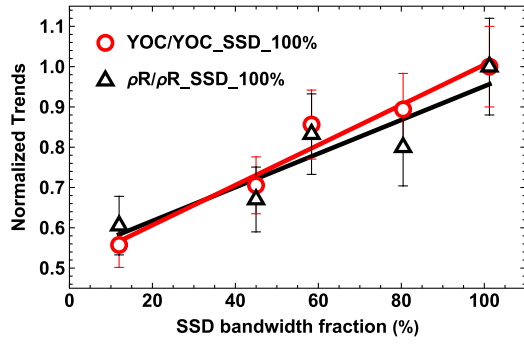

FIG. 3. Trends in measured YOC (in open red circles) and areal density (in open black triangles) as SSD bandwidth is varied in for $\alpha_F \simeq 5$ implosions. Least-square fit with a plateau above 40% SSD is shown as solid lines. All data normalized to 100% SSD experiment.

FIG. 4. Trends in measured YOC (in open red circles) and areal density (in open black triangles) as SSD bandwidth is varied for $\alpha_F \simeq 3.5$ implosions. Least-square fit to the data (shown as solid lines) indicates trends are statistically significant with reduced χ^2 of 1.12 and 0.97, respectively. All data normalized to 100% SSD experiment.

from laser imprinting. Unlike the $\alpha_F \simeq 5$ implosions (Fig. 3), the lower adiabat $\alpha_F \simeq 3.5$ implosions (Fig. 4) would benefit from higher bandwidth (than presently available on OMEGA) in both yields and areal densities.

Additionally, other core properties were measured as a function of bandwidth. All these measurements, described in the Supplemental Material [53], corroborate the behavior of performance metrics for both $\alpha_F \simeq 5$ SSD-scan (insensitive to bandwidth at 100% SSD) and $\alpha_F \simeq 3.5$ SSD-scan (sensitive to bandwidth up to 100% SSD). Note, that changes in SSD bandwidth (besides laser-imprinting) also change the behavior of laser-plasma instabilities [58–60] (primarily CBET and two-plasmon-decay), which may impact implosion performance. However, measured absorption [61] and hard x-ray (HXR) data [62] indicate that the effects of the SSD bandwidth on these instabilities are minimal (except the lowest of SSD bandwidths below 20%, where modestly enhanced HXR emission is observed). See the Supplemental Material [53] for the details. Note also that, if laser-plasma instabilities are driving the trends with SSD bandwidth for $\alpha_F \simeq 3.5$ implosions, then even $\alpha_F \simeq 5$ implosions should show similar trends. This leaves laser imprinting as the main physical mechanism driving the trends in Fig. 4.

To infer performance improvements achievable with future-generation ultra-broadband lasers [30,31], we extrapolate the measured trends beyond 100% SSD. This is done using both a power law fit to the data and simulations. Note that the σ_{rms} of overlapped nonuniformity is the physical quantity determining yield degradation. Since, σ_{rms} is a nonlinear function of SSD bandwidth, we first determine YOC's dependence on σ_{rms} and subsequently convert σ_{rms} to SSD bandwidth. Also, the lowest SSD bandwidth data point is excluded from the fits as we are interested in behavior close to 100% SSD. The same procedure is used to extrapolate ρR. Figure 5 shows the YOC and ρR improvements predicted for higher SSD
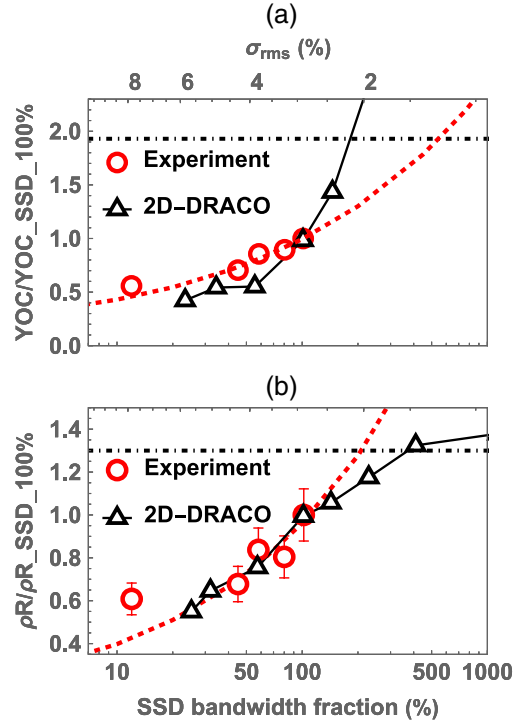

FIG. 5. Performance extrapolation to higher bandwidth using power law least-square fits for $\alpha_F \simeq 3.5$ implosions: (a) Extrapolation of YOC. (b) Extrapolation of areal density. Top axis shows corresponding σ_{rms} values. Open red circles show the measured data. Open black triangles show results from 2D-DRACO simulations described in [64,65]. Black dot-dashed lines show upper bounds on achievable improvements based on results from $\alpha_F \simeq 5$ SSD scan.

bandwidths using power-law extrapolations of the data (red dashed). We also compare them to 2D DRACO [63] simulations of similar low-adiabat targets described in [64,65]. In these simulations, imprinting levels are varied using a multiplier to the imprint spectrum, and the nominal 100% SSD σ_{rms} is augmented by 1.5× from tuning 2D simulations with dedicated mix experiments [27] (see the Supplemental Material [53]). Since there is significant performance degradation even for the imprint insensitive $\alpha_F \simeq 5$ 100% SSD bandwidth implosions, caused by presently unexplained 1D/3D physics, we use measured YOC and $\rho R/\rho R_{1D}$ of $\alpha \simeq 5$ 100% SSD bandwidth implosions, as the maximum achievable YOC and $\rho R/\rho R_{1D}$ for $\alpha \simeq 3.5$ implosions (dot-dashed lines in Fig. 5). Using the lowest extrapolated values [red dashed in Fig. 5(a), solid black in Fig. 5(b)], an improvement of $\approx 1.9\times$ in yields and $\approx 1.3\times$ in areal densities can be expected with ultra-broadband lasers with $\approx 6\times$ the current OMEGA bandwidth. Note that $\alpha_F \simeq 3.5$ adiabat is an optimistic upper limit on the adiabat required for high-gain fusion. However, in reality, adiabats $\alpha_F \simeq 1$–2 may be needed, and the requisite improvement may be higher than 6×. This bandwidth extrapolation implies

$\approx 3\times$ reduction in nonuniformity σ_{rms}. Note that improvements at higher bandwidth shown in Fig. 5 refer only to imprint mitigation and do not include the expected enhancement in energy coupling and suppression of laser-plasma instabilities [66,67], which would further improve implosion performance.

In summary, the sensitivity of the performance of OMEGA cryogenic implosions to SSD bandwidth was studied to assess the role of laser imprinting in high performance DT-layered implosions with different in-flight stability characteristics. $\alpha_F \simeq 5$ design was found to be insensitive to imprinting at maximum bandwidth. Instead $\alpha_F \simeq 3.5$ designs were found to be sensitive to laser imprinting up to full bandwidth. These results corroborate conclusions from statistical modeling, which show significant degradation from short-scale perturbations for $\alpha_F \simeq 3.5$ design but not for $\alpha_F \simeq 5$ design. These experiments indicate that the dominant source of short-scale perturbations degrading $\alpha_F \simeq 3.5$ implosions is laser imprinting. Based on extrapolation of the measured data, significant improvement in performance is expected for next-generation broadband ICF lasers [30,31].

[1] J. Nuckolls, L. Wood, A. Thiessen, and G. Zimmerman, Laser compression of matter to super-high densities: Thermonuclear (CTR) applications, Nature (London) **239**, 139 (1972).

[2] R. Betti and O. Hurricane, Inertial-confinement fusion with lasers, Nat. Phys. **12**, 435 (2016).

[3] S. Atzeni and J. Meyer-Ter-Vehn, *The Physics of Inertial Fusion* (Oxford University Press, Oxford, UK, 2004).

[4] R. S. Craxton, K. S. Anderson, T. R. Boehly, V. N. Goncharov, D. R. Harding, J. P. Knauer, R. L. McCrory, P. W. McKenty, D. D. Meyerhofer, J. F. Myatt *et al.*, Direct-drive inertial confinement fusion: A review, Phys. Plasmas **22**, 110501 (2015).

[5] L. Rayleigh, Proc. London Math. Soc. **s1-15**, 69 (1883).

[6] J. D. Kilkenny, S. G. Glendinning, S. W. Haan, B. A. Hammel, J. D. Lindl, D. Munro, B. A. Remington, S. V. Weber, J. P. Knauer, and C. P. Verdon, A review of the ablative stabilization of the Rayleigh–Taylor instability in regimes relevant to inertial confinement fusion, Phys. Plasmas **1**, 1379 (1994).

[7] John H. Gardner and Stephen E. Bodner, Wavelength Scaling for Reactor-Size Laser-Fusion Targets, Phys. Rev. Lett. **47**, 1137 (1981).

[8] R. Ishizaki and K. Nishihara, Model of hydrodynamic perturbation growth in the start-up phase of laser implosion, Phys. Rev. E **58**, 3744 (1998).

[9] V. N. Goncharov, S. Skupsky, T. R. Boehly, J. P. Knauer, P. McKenty, V. A. Smalyuk, R. P. J. Town, and O. V. Gotchev, A model of laser imprinting, Phys. Plasmas **7**, 2062 (2000).

[10] Y. Kato, K. Mima, N. Miyanaga, S. Arinaga, Y. Kitagawa, M. Nakatsuka, and C. Yamanaka, Random Phasing of High-Power Lasers for Uniform Target Acceleration and Plasma-Instability Suppression, Phys. Rev. Lett. **53**, 1057 (1984).

[11] H. Azechi, M. Nakai, K. Shigemori, N. Miyanaga, H. Shiraga, H. Nishimura, M. Honda, R. Ishizaki, J. G. Wouchuk, H. Takabe *et al.*, Direct-drive hydrodynamic instability experiments on the GEKKO XII laser, Phys. Plasmas **4**, 4079 (1997).

[12] S. Skupsky, R. W. Short, T. Kessler, R. S. Craxton, S. Letzring, and J. M. Soures, Improved laser-beam uniformity using the angular dispersion of frequency-modulated light, J. Appl. Phys. **66**, 3456 (1989).

[13] S. Skupsky and R. S. Craxton, Irradiation uniformity for high-compression laser-fusion experiments, Phys. Plasmas **6**, 2157 (1999).

[14] T. J. Kessler, Y. Lin, J. J. Armstrong, and B. Velazquez, Laser coherence control: Technology and applications, Proc. SPIE Int. Soc. Opt. Eng. **1870**, 95 (1993).

[15] R. H. Lehmberg and S. P. Obenschain, Use of induced spatial incoherence for uniform illumination of laser fusion targets, Opt. Commun. **46**, 27 (1983).

[16] R. H. Lehmberg, A. J. Schmitt, and S. E. Bodner, Theory of induced spatial incoherence, J. Appl. Phys. **62**, 2680 (1987).

[17] S. P. Obenschain, J. Grun, M. J. Herbst, K. J. Kearney, C. K. Manka, E. A. McLean *et al.*, Laser-Target Interaction with Induced Spatial Incoherence, Phys. Rev. Lett. **56**, 2807 (1986).

[18] J. E. Rothenberg, Comparison of beam-smoothing methods for direct-drive inertial confinement fusion, J. Opt. Soc. Am. B **14**, 1664 (1997).

[19] Y. Lin, T. J. Kessler, and G. N. Lawrence, Design of continuous surface-relief phase plates by surface-based simulated annealing to achieve control of focal-plane irradiance, Opt. Lett. **21**, 1703 (1996).

[20] S. E. Bodner, D. G. Colombant, J. H. Gardner, R. H. Lehmberg, S. P. Obenschain, L. Phillips, A. J. Schmitt, J. D. Sethian, R. L. McCrory, W. Seka *et al.*, Direct-drive laser fusion: Status and prospects, Phys. Plasmas **5**, 1901 (1998).

[21] Sean P. Regan, John A. Marozas, John H. Kelly, Thomas R. Boehly, William R. Donaldson, Paul A. Jaanimagi, Robert L. Keck, Terrance J. Kessler, David D. Meyerhofer, Wolf Seka *et al.*, Experimental investigation of smoothing by spectral dispersion, J. Opt. Soc. Am. B **17,** 1483 (2000).

[22] T. R. Boehly, V. A. Smalyuk, D. D. Meyerhofer, J. P. Knauer, D. K. Bradley, R. S. Craxton, M. J. Guardalben, S. Skupsky, and T. J. Kessler, Reduction of laser imprinting using polarization smoothing on a solid-state fusion laser, J. Appl. Phys. **85,** 3444 (1999).

[23] V. A. Smalyuk, O. Sadot, J. A. Delettrez, D. D. Meyerhofer, S. P. Regan, and T. C. Sangster, Fourier-Space Nonlinear Rayleigh-Taylor Growth Measurements of 3D Laser-Imprinted Modulations in Planar Targets, Phys. Rev. Lett. **95,** 215001 (2005).

[24] V. A. Smalyuk, S. X. Hu, V. N. Goncharov, D. D. Meyerhofer, T. C. Sangster, C. Stoeckl, and B. Yaakobi, Systematic study of Rayleigh–Taylor growth in directly driven plastic targets in a laser-intensity range from $\sim 2 \times 10^{14}$ to $\sim 1.5 \times 10^{15}$ W/cm^2, Phys. Plasmas **15,** 082703 (2008).

[25] A. Casner, L. Masse, B. Delorme, D. Martinez, G. Huser, D. Galmiche, S. Liberatore, I. Igumenshchev, M. Olazabal-Loumé, Ph. Nicolaï *et al.*, Progress in indirect and direct-drive planar experiments on hydrodynamic instabilities at the ablation front, Phys. Plasmas **21,** 122702 (2014).

[26] V. A. Smalyuk, S. X. Hu, J. D. Hager, J. A. Delettrez, D. D. Meyerhofer, T. C. Sangster, and D. Shvarts, Rayleigh-Taylor Growth Measurements in the Acceleration Phase of Spherical Implosions on OMEGA, Phys. Rev. Lett. **103,** 105001 (2009).

[27] T. J. B. Collins, C. Stoeckl, R. Epstein, W. A. Bittle, C. J. Forrest, V. Yu. Glebov, V. N. Goncharov, D. R. Harding, S. X. Hu, D. W. Jacobs-Perkins *et al.*, Causes of fuel–ablator mix inferred from modeling of monochromatic time-gated radiography of OMEGA cryogenic implosions, Phys. Plasmas **29,** 012702 (2022).

[28] S. X. Hu, D. T. Michel, A. K. Davis, R. Betti, P. B. Radha, E. M. Campbell, D. H. Froula, and C. Stoeckl, Understanding the effects of laser imprint on plastic-target implosions on OMEGA, Phys. Plasmas **23,** 102701 (2016).

[29] Sean P. Regan, John A. Marozas, R. Stephen Craxton, John H. Kelly, William R. Donaldson, Paul A. Jaanimagi, Douglas Jacobs-Perkins, Robert L. Keck, Terrance J. Kessler, David D. Meyerhofer *et al.*, Performance of 1-THz-bandwidth, two-dimensional smoothing by spectral dispersion and polarization smoothing of high-power, solid-state laser beams, J. Opt. Soc. Am. B **22,** 998 (2005).

[30] C. Dorrer, E. M. Hill, and J. D. Zuegel, High-energy parametric amplification of spectrally incoherent broadband pulses, Opt. Express **28,** 451 (2020).

[31] S. P. Obenschain, A. J. Schmitt, J. W. Bates, M. F. Wolford, M. C. Myers, M. W. McGeoch, M. Karasik, and J. L. Weaver, Direct drive with the argon fluoride laser as a path to high fusion gain with sub-megajoule laser energy, Phil. Trans. R. Soc. A **378,** 2184 (2020).

[32] Max Karasik, Jaechul Oh, S. P. Obenschain, A. J. Schmitt, Y. Aglitskiy, and C. Stoeckl, Order-of-magnitude laser imprint reduction using pre-expanded high-Z coatings on targets driven by a third harmonic Nd:glass laser, Phys. Plasmas **28,** 032710 (2021).

[33] S. X. Hu, W. Theobald, P. B. Radha, J. L. Peebles, S. P. Regan, A. Nikroo, M. J. Bonino, D. R. Harding, V. N. Goncharov, N. Petta, T. C. Sangster, and E. M. Campbell, Mitigating laser-imprint effects in direct-drive inertial confinement fusion implosions with an above-critical-density foam layer, Phys. Plasmas **25,** 082710 (2018).

[34] V. Gopalaswamy, R. Betti, J. P. Knauer, N. Luciani, D. Patel, K. M. Woo, A. Bose *et al.*, Tripled yield in direct-drive laser fusion through statistical modelling, Nature (London) **565,** 581 (2019).

[35] R. Betti, A. R. Christopherson, B. K. Spears, R. Nora, A. Bose, J. Howard, K. M. Woo, M. J. Edwards, and J. Sanz, Alpha Heating and Burning Plasmas in Inertial Confinement Fusion, Phys. Rev. Lett. **114,** 255003 (2015).

[36] A. R. Christopherson, R. Betti, S. Miller, V. Gopalaswamy, O. Mannion, and D. Cao, Theory of ignition and burn propagation in inertial fusion implosions, Phys. Plasmas **27,** 052708 (2020).

[37] J. D. Lindl, S. W. Haan, O. L. Landen, A. R. Christopherson, and R. Betti, Progress toward a self-consistent set of 1D ignition capsule metrics in ICF, Phys. Plasmas **25,** 122704 (2018).

[38] A. R. Christopherson, R. Betti, and J. D. Lindl, Thermonuclear ignition and the onset of propagating burn in inertial fusion implosions, Phys. Rev. E **99,** 021201(R) (2019).

[39] J. Delettrez, R. Epstein, M. C. Richardson, P. A. Jaanimagi, and B. L. Henke, Effect of laser illumination nonuniformity on the analysis of time-resolved x-ray measurements in uv spherical transport experiments, Phys. Rev. A **36,** 3926 (1987).

[40] C. J. Randall, J. J. Thomson, and K. G. Estabrook, Enhancement of Stimulated Brillouin Scattering due to Reflection of Light from Plasma Critical Surface, Phys. Rev. Lett. **43,** 924 (1979).

[41] J. A. Marozas and T. J. B. Collins, Cross-beam energy transfer (CBET) effect integrated into the 2-D hydrodynamics code DRACO, Bull. Am. Phys. Soc. **57,** 344 (2012).

[42] V. N. Goncharov, T. C. Sangster, P. B. Radha, R. Betti, T. R. Boehly, T. J. B. Collins, R. S. Craxton, J. A. Delettrez, R. Epstein, V. Yu. Glebov *et al.*, Performance of direct-drive cryogenic targets on OMEGA, Phys. Plasmas **15,** 056310 (2008).

[43] S. X. Hu, V. N. Goncharov, P. B. Radha, J. A. Marozas, S. Skupsky, T. R. Boehly, T. C. Sangster, D. D. Meyerhofer, and R. L. McCrory, Two-dimensional simulations of the neutron yield in cryogenic deuterium-tritium implosions on OMEGA, Phys. Plasmas **17,** 102706 (2010).

[44] A. Lees, R. Betti, J. P. Knauer, V. Gopalaswamy, D. Patel, K. M. Woo, K. S. Anderson, E. M. Campbell, D. Cao, J. Carroll-Nellenback *et al.*, Experimentally Inferred Fusion Yield Dependencies of OMEGA Inertial Confinement Fusion Implosions, Phys. Rev. Lett. **127,** 105001 (2021).

[45] K. M. Woo, R. Betti, O. M. Mannion, C. J. Forrest, J. P. Knauer, V. N. Goncharov, P. B. Radha, D. Patel, V. Gopalaswamy, and V. Y. Glebov, Inferring thermal ion temperature and residual kinetic energy from nuclear measurements in inertial confinement fusion implosions, Phys. Plasmas **27,** 062702 (2020).

[46] C. J. Forrest, P. B. Radha, V. Yu. Glebov, V. N. Goncharov, J. P. Knauer, A. Pruyne, M. Romanofsky, T. C. Sangster, M. J. Shoup III, C. Stoeckl *et al.*, High-resolution spectroscopy used to measure inertial confinement fusion neutron spectra on Omega, Rev. Sci. Instrum. **83,** 10D919 (2012).

[47] V. Yu. Glebov, C. J. Forrest, K. L. Marshall, M. Romanofsky, T. C. Sangster, M. J. Shoup III, and C. Stoeckl, A new neutron time-of-flight detector for fuel-areal-density measurements on OMEGA, Rev. Sci. Instrum. **85,** 11E102 (2014).

[48] D. T. Casey, J. A. Frenje, M. Gatu Johnson, F. H. Séguin, C. K. Li, R. D. Petrasso, V. Yu. Glebov, J. Katz, J. Magoon, D. D. Meyerhofer *et al.*, The magnetic recoil spectrometer for measurements of the absolute neutron spectrum at OMEGA and the NIF, Rev. Sci. Instrum. **84,** 043506 (2013).

[49] J. A. Frenje, R. Bionta, E. J. Bond, J. A. Caggiano, D. T. Casey, C. Cerjan, J. Edwards, M. Eckart, D. N. Fittinghoff, S. Friedrich *et al.*, Diagnosing implosion performance at the National Ignition Facility (NIF) by means of neutron spectrometry, Nucl. Fusion **53,** 043014 (2013).

[50] F. J. Marshall, R. E. Bahr, V. N. Goncharov, V. Yu. Glebov, B. Peng, S. P. Regan, T. C. Sangster, and C. Stoeckl, A framed, 16-image Kirkpatrick–Baez x-ray microscope, Rev. Sci. Instrum. **88,** 093702 (2017).

[51] V. N. Goncharov, T. C. Sangster, R. Betti, T. R. Boehly, M. J. Bonino, T. J. B. Collins, R. S. Craxton, J. A. Delettrez, D. H. Edgell, R. Epstein *et al.*, Improving the hot-spot pressure and demonstrating ignition hydrodynamic equivalence in cryogenic deuterium–tritium implosions on OMEGA, Phys. Plasmas **21,** 056315 (2014).

[52] Huasen Zhang, R. Betti, Rui Yan, and H. Aluie, Nonlinear bubble competition of the multimode ablative Rayleigh–Taylor instability and applications to inertial confinement fusion, Phys. Plasmas **27,** 122701 (2020).

[53] See Supplemental Material at http://link.aps.org/supplemental/10.1103/PhysRevLett.131.105101 for (Sec. 2) the theoretical analysis of dependence of YOC on adiabat; (Sec. 1) for the relationship between SSD bandwidth fraction and nonuniformity; (Sec. 4) for the measured trends in core properties with SSD bandwidth variation; (Sec. 5) for the effects of bandwidth on CBET and TPD; (Sec. 3) for the YOC and areal density trends from 2D-DRACO simulations, which includes Refs. [54,55].

[54] V. Yu. Glebov, D. D. Meyerhofer, C. Stoeckl, and J. D. Zuegel, Secondary-neutron-yield measurements by current-mode detectors, Rev. Sci. Instrum. **72,** 824 (2001).

[55] C. Stoeckl, R. Boni, F. Ehrne, C. J. Forrest, V. Yu. Glebov, J. Katz, D. J. Lonobile, J. Magoon, S. P. Regan *et al.*, Neutron temporal diagnostic for high-yield deuterium-tritium cryogenic implosions on OMEGA, Rev. Sci. Instrum. **87,** 053501 (2016).

[56] D. R. Harding and W. T. Shmayda, Stress- and radiation-induced swelling in plastic capsules, Fusion Sci. Technol. **63,** 125 (2013).

[57] W. R. Donaldson, M. Millecchia, and R. keck, A multi-channel, high-resolution, UV spectrometer for laser-fusion applications, Rev. Sci. Instrum. **76,** 073106 (2005).

[58] A. G. Seaton, L. Yin, R. K. Follett, B. J. Albright, and A. Le, Cross-beam energy transfer in direct-drive ICF. II. Theory and simulation of mitigation through increased laser bandwidth, Phys. Plasmas **29,** 042707 (2022).

[59] R. K. Follett, A. Colaïtis, A. G. Seaton, H. Wen, D. Turnbull, D. H. Froula, and J. P. Palastro, Ray-based cross-beam energy transfer modeling for broadband lasers, Phys. Plasmas **30,** 042102 (2023).

[60] D. Turnbull, A. V. Maximov, D. Cao, A. R. Christopherson, D. H. Edgell, R. K. Follett, V. Gopalaswamy, J. P. Knauer, J. P. Palastro, A. Shvydky, C. Stoeckl, H. Wen, and D. H. Froula, Impact of spatiotemporal smoothing on the two-plasmon–decay instability, Phys. Plasmas **27,** 102710 (2020).

[61] W. Seka, D. H. Edgell, J. P. Knauer, J. F. Myatt, A. V. Maximov, R. W. Short, T. C. Sangster, C. Stoeckl, R. E. Bahr, R. S. Craxton, J. A. Delettrez, V. N. Goncharov, I. V. Igumenshchev, and D. Shvarts, Time-resolved absorption in cryogenic and room-temperature direct-drive implosions, Phys. Plasmas **15,** 056312 (2008).

[62] C. Stoeckl, V. Yu. Glebov, D. D. Meyerhofer, W. Seka, B. Yaakobi, R. P. J. Town, and J. D. Zuegel, Hard x-ray detectors for OMEGA and NIF, Rev. Sci. Instrum. **72,** 1197 (2001).

[63] P. B. Radha, T. J. B. Collins, J. A. Delettrez, Y. Elbaz, R. Epstein, V. Yu. Glebov, V. N. Goncharov, R. L. Keck, J. P. Knauer, J. A. Marozas *et al.*, Multidimensional analysis of direct-drive, plastic-shell implosions on OMEGA, Phys. Plasmas **12,** 056307 (2005).

[64] R. Nora, R. Betti, K. S. Anderson, A. Shvydky, A. Bose, K. M. Woo, A. R. Christopherson, J. A. Marozas, T. J. B. Collins, P. B. Radha *et al.*, Theory of hydro-equivalent ignition for inertial fusion and its applications to OMEGA and the National Ignition Facility, Phys. Plasmas **21,** 056316 (2014).

[65] R. Nora, Ph.D. thesis, University of Rochester, 2015, http://hdl.handle.net/1802/29713.

[66] J. W. Bates, R. K. Follett, J. G. Shaw, S. P. Obenschain, R. H. Lehmberg, J. F. Myatt, J. L. Weaver, D. M. Kehne, M. F. Wolford, and M. C. Myers, Suppressing cross-beam energy transfer with broadband lasers, High Energy Density Phys. **36,** 100772 (2020).

[67] R. K. Follett, J. G. Shaw, J. F. Myatt, H. Wen, D. H. Froula, and J. P. Palastro, Thresholds of absolute two-plasmon-decay and stimulated Raman scattering instabilities driven by multiple broadband lasers, Phys. Plasmas **28,** 032103 (2021).